THE JOURNAL OF PHYSICAL CHEMISTRY A

Article

pubs.acs.org/JPCA

Experimental and Theoretical Investigations of the Dissociation Energy (D_0) and Dynamics of the Water Trimer, $(H_2O)_3$

Lee C. Ch'ng,[†] Amit K. Samanta,[†] Yimin Wang,[‡] Joel M. Bowman,*[,‡] and Hanna Reisler*[,†]

[†]Department of Chemistry, University of Southern California, Los Angeles, California 90089, United States

[‡]Department of Chemistry and Cherry L. Emerson Center for Scientific Computation, Emory University, Atlanta, Georgia 30322, United States

W *Web-Enhanced Feature* *S* *Supporting Information*

ABSTRACT: We report a joint experimental-theoretical study of the predissociation dynamics of the water trimer following excitation of the hydrogen bonded OH-stretch fundamental. The bond dissociation energy (D_0) for the $(H_2O)_3 \rightarrow H_2O + (H_2O)_2$ dissociation channel is determined from fitting the speed distributions of selected rovibrational states of the water monomer fragment using velocity map imaging. The experimental value, $D_0 = 2650 \pm 150$ cm^{-1}, is in good agreement with the previously determined theoretical value, 2726 ± 30 cm^{-1}, obtained using an ab initio full-dimensional potential energy surface (PES) together with Diffusion Monte Carlo calculations [Wang; Bowman. *J. Chem. Phys.* **2011**, *135*, 131101]. Comparing this value to D_0 of the dimer places the contribution of nonpairwise additivity to the hydrogen bonding at 450−500 cm^{-1}. Quasiclassical trajectory (QCT) calculations using this PES help elucidate the reaction mechanism. The trajectories show that most often one hydrogen bond breaks first, followed by breaking and re-forming of hydrogen bonds (often with different hydrogen bonds breaking) until, after many picoseconds, a water monomer is finally released. The translational energy distributions calculated by QCT for selected rotational levels of the monomer fragment agree with the experimental observations. The product translational and rotational energy distributions calculated by QCT also agree with statistical predictions. The availability of low-lying intermolecular vibrational levels in the dimer fragment is likely to facilitate energy transfer before dissociation occurs, leading to statistical-like product state distributions.

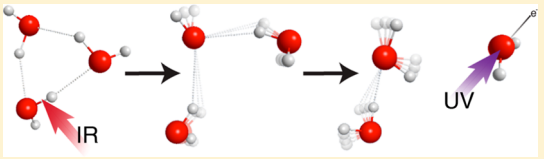

INTRODUCTION

Since the first description of the hydrogen bond (H-bond) in water in the early 1920s, the study of water has been an area of intense research efforts.[1−6] Water and its H-bond network is an exceedingly complicated system that is still not understood completely. The unique properties of water, such as its unusual density and high boiling point, are mainly due to the intermolecular forces that act among water molecules both in pairwise and nonpairwise additive interactions. As the smallest water cluster with a complete H-bond network, the cyclic water trimer serves as a prototype for examination of cooperative (nonadditive) interactions. This can help to understand the complex nature of larger water networks, such as liquids, solids, water chains, etc.

The structure, vibrational frequencies, potential energy surface (PES), three-body effects, binding energies, and tunneling motions of the water trimer have been studied extensively by theory.[7−12] Work up to 2003 is summarized in an exhaustive review,[12] and additional work has been published since then.[13−19] In gas phase experiments, emphasis has been placed on investigations of the trimer in cold molecular beams, with most reports focusing on structure and spectroscopy. In particular, the detailed, high-resolution spectroscopic studies of Saykally and co-workers mapped the vibrational, rotational, and tunneling (VRT) states of the trimer and estimated the barriers between different conformations.[12,20] In addition, the intra- and intermolecular vibrational modes were characterized in molecular beams, He droplets and matrix isolation experiments.[21−29]

Despite the fundamental interest in the nature of the cooperative interactions in the H-bond network and their influence on the H-bond strength,[6,7,12,30−33] no experimental measurements of the dissociation energy (D_0) of the trimer have been reported. Likewise, studies of energy transfer and H-bond breaking pathways of water clusters are scarce, partly because of difficulties in detecting water fragments. Our recent success in detecting internally excited water fragments in the vibrational predissociation (VP) of the water dimer paved the way for studying bond breaking in larger water clusters. Recently, D_0 of the water dimers $(H_2O)_2$ and $(D_2O)_2$, whose binding is dominated by pairwise interactions, were determined accurately at 1105 and 1244 ± 10 cm^{-1},[34,35] respectively, in excellent agreement with the corresponding calculated values of 1104 and 1244 ± 5 cm^{-1}.[36,37] Quasiclassical trajectory (QCT) calculations using an accurate full-dimensional PES were in accord with the experiments and helped to elucidate

Special Issue: Joel M. Bowman Festschrift

Received: January 31, 2013
Revised: March 26, 2013

   dx.doi.org/10.1021/jp401155v | *J. Phys. Chem. A* XXXX, XXX, XXX−XXX

dissociation mechanisms.[35] Due to the larger number of available fragment quantum states, experimental investigations of $(H_2O)_3$ are much more challenging.

The excellent agreement between theory and experiment for D_0 of the water dimer has defined this system as a benchmark for theory. Subsequently, Wang and Bowman[38] calculated D_0 of $(H_2O)_3$ and $(D_2O)_3$ using an ab initio full-dimensional PES together with diffusion Monte Carlo calculations. The calculated D_0 values for the $(H_2O)_3 \rightarrow H_2O + (H_2O)_2$ and $(H_2O)_3 \rightarrow 3H_2O$ dissociation channels are 2726 ± 30 and 3855 ± 20 cm^{-1}, respectively.[38] The issue of nonpairwise additivity was investigated theoretically and its contribution to the value obtained by simply doubling the dimer's D_0 ($1105 \times 2 = 2210$ cm^{-1}) was estimated at about 500 cm^{-1}. An experimental confirmation of the cooperative interaction modeled by theory is highly desirable. An agreement would also help to increase the confidence level for calculations of higher clusters with similar types of H-bond networks.

In this contribution we report the first experimental determination of D_0 of $(H_2O)_3$ by exciting the H-bonded OH-stretch fundamental at 3536 cm^{-1}. We can obtain D_0 only for the $H_2O + (H_2O)_2$ channel, as the excitation energy is insufficient to break all three H-bonds. We also examine the *pair-correlated* fragment state distributions, i.e., the $(H_2O)_2$ cofragment (undetected fragment) state distribution correlated with a *specific* rotational state of the monitored H_2O fragment. Following excitation of the H-bonded OH-stretch of $(H_2O)_3$, H_2O fragments can be formed only in the ground vibrational state, whereas all the intermolecular vibrational modes of the $(H_2O)_2$ fragment can be populated (but not the intramolecular modes).

Our previous experimental and theoretical investigations of energy transfer in the water dimer found predominant bending excitation in the monomer fragment upon H-bond breaking. A preference for final fragment rotational states that minimize translational energy release was also observed. Because the H_2O fragment bending excitation is energetically forbidden in VP of $(H_2O)_3$ via excitation of the H-bonded OH-stretch, vibrational population can only reside in the intermolecular modes of $(H_2O)_2$. Due to the large density of states in the $(H_2O)_2$ fragment, its energy distributions might be more statistical compared to the corresponding behavior in fragments of $(H_2O)_2$ dissociation and other small water-containing dimers.[34,35,39−41] The energy distributions in the trimer's fragmentation are compared here to the results of QCT calculations and statistical predictions.

The water trimer adopts six low-lying stationary points (Figure 1). Among these, the global minimum consists of three H-bonds and has a cyclic structure that is conventionally denoted as "up−up−down" depending on the orientations of the free OH-bonds relative to the plane defined by the three oxygen atoms.[12,42] $(H_2O)_3$ has one weaker H-bond due to repulsion of the two "up" OH-bonds, giving two different H-bonded OH-stretch fundamentals that differ in energy by 12−15 cm^{-1}.[19,28]

EXPERIMENTAL METHODS

Vibrational predissociation of $(H_2O)_3$ formed in a pulsed supersonic molecular beam was studied following pulsed infrared (IR) laser excitation. Two experimental methods of data collection were used: (i) time-of-flight mass spectrometry combined with 2 + 1 resonance-enhanced multiphoton ionization (REMPI) for spectroscopic investigations of H_2O fragments and (ii) velocity map imaging (VMI) for deriving internal energy distributions of $(H_2O)_2$ cofragments (undetected fragments) as well as determining D_0 for the $(H_2O)_3 \rightarrow H_2O + (H_2O)_2$ channel. Figure 2 illustrates the experimental scheme. Upon excitation of the H-bonded OH-stretch, VP occurs following coupling of energy to the dissociation coordinate. The excess energy can be distributed among center-of-mass (c.m.) translation and rotational and rovibrational states of the H_2O and $(H_2O)_2$ fragments, respectively.

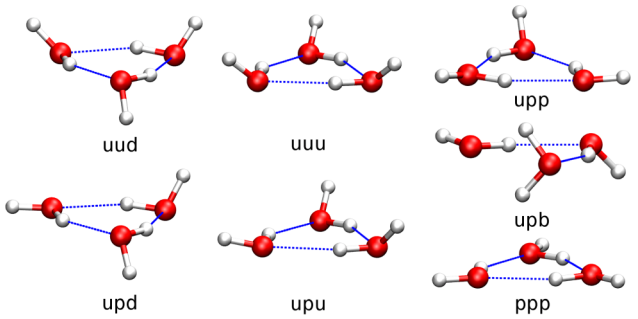

Figure 1. Configurations of the up−up−down (uud) global minimum and other low-lying stationary points of the water trimer. See ref 42 for the energies of these stationary points, which are less than 1 kcal/mol (350 cm^{-1}) above the global minimum except for the planar ppp saddle point.

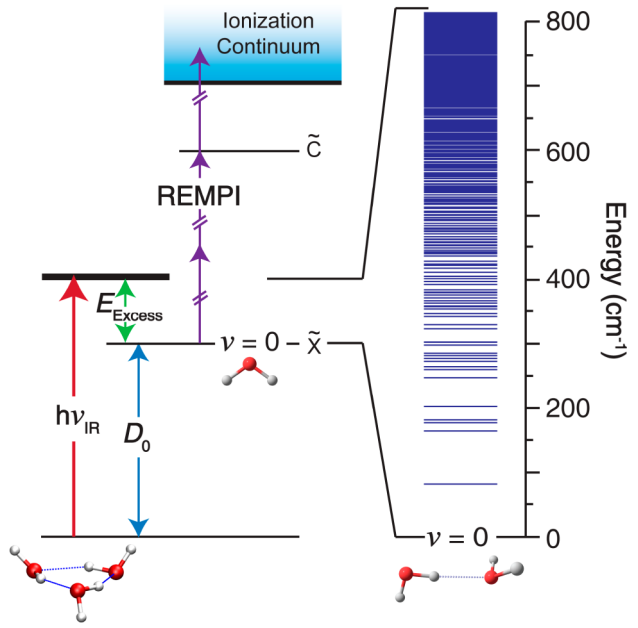

Figure 2. Experimental scheme for vibrational predissociation of $(H_2O)_3$. An IR photon ($h\nu_{IR}$) excites the H-bonded OH-stretch of $(H_2O)_3$. Some of the excess energy (E_{Excess}) can be distributed in intermolecular vibrational levels (fundamentals, overtones, and combination bands) of $(H_2O)_2$. Blue horizontal lines show the vibrational states of the dimer fragment (calculated using harmonic approximation and published vibrational frequencies)[43] as a function of excess energy. H_2O fragments in the ground vibrational state are detected by REMPI via the C̃ state.

The experimental procedures are similar to those used in previous studies.[35,39−41] $(H_2O)_3$ was formed in a pulsed supersonic molecular beam by expanding ~1% water in helium (Gilmore, 99.9999%) at a stagnation pressure of 1.4 atm through the 0.5 mm orifice of a pulsed valve (~150 μs opening

dx.doi.org/10.1021/jp401155v | J. Phys. Chem. A XXXX, XXX, XXX−XXX

time) operating at 10 Hz. Samples were prepared by transferring H_2O by vacuum distillation to an evacuated reservoir followed by adding helium. Expansion conditions (water concentration, helium backing pressure) were optimized to maximize signal from the trimer and minimize higher clusters. The skimmed molecular beam was intersected at right angles by two counter-propagating laser beams in the interaction region. IR radiation (5 mJ/pulse, ~0.4 cm^{-1} line width) excited the H-bonded OH-stretch of $(H_2O)_3$ at 3536 cm^{-1}. Focusing the IR radiation increases the enhancement from multiphoton absorption of higher clusters and therefore was avoided in this experiment.[41] IR radiation was generated by an optical parametric oscillator/amplifier (OPO/OPA) system (LaserVision) pumped by the fundamental of a seeded Nd:YAG laser (Continuum Precision II 8000). The IR frequency was calibrated by measuring the well-known absorption spectrum of gaseous H_2O.

Ultraviolet (UV) radiation at 248.24−248.55 nm was generated by frequency-doubling (Inrad Autotracker III) the output of the dye laser (Continuum ND 6000, Coumarin 500) pumped by a Nd:YAG laser (Continuum Surelite III) and frequency calibrated by the known REMPI spectrum of H_2O.[44] Tightly focused UV radiation (0.4−0.6 mJ/pulse, lens focal length (fl) = 20 cm; ~0.4 cm^{-1} line width) ionized state-selected H_2O fragment, scanning through the $\tilde{C}\ ^1B_1(000) \leftarrow \tilde{X}\ ^1A_1(000)$ band using REMPI. Tighter focusing of the UV beam was achieved by expanding it using an additional negative lens (fl = −100 cm) placed 137 cm before the focusing lens. Spectra were collected by alternating "IR on" and "IR off" conditions at each frequency. In "IR on", the IR laser was fired 70 ns before the UV laser. The REMPI spectra were simulated using the program PGOPHER[45] with rotational constants from Yang et al.[44] IR laser conditions (timing, focusing, power) were optimized to ensure single-photon absorption. UV laser conditions were optimized for the best signal-to-noise ratio. The timing of the lasers was adjusted by delay generators (Stanford, DG535) controlled through a GPIB interface (National Instruments). A cryopumping system cooled by liquid nitrogen served to reduce background water during data acquisition.

The VMI arrangement has been described in detail previously.[46,47] In brief, it consists of a four-electrode ion acceleration assembly, a 60 cm field-free drift tube, and a microchannel plate (MCP) detector coupled to a phosphor screen (Beam Imaging Solutions, Inc. BOS-40-6) that is monitored by a charge-coupled device (CCD) camera (LaVision, Imager). In the VMI mode, the two-dimensional projections were collected using an event counting method (DaVis) and reconstructed to three-dimensional images using the BASEX method.[48] Speed distributions were obtained by summing over the angular distribution for each radius, and were converted to c.m. translational energy distributions using momentum conservation, the appropriate Jacobian (proportional to $E_T^{-1/2}$, where E_T is the translational energy) and calibration constants obtained from previous calibration experiments.[39]

THEORETICAL METHODS

Quasiclassical trajectories were run essentially as described previously for analogous predissociation studies of the water dimer.[35] Initial conditions were expressed in the normal modes of the trimer by giving harmonic zero-point energy (ZPE) to each mode, except for the IR-bright H-bonded OH-stretch. That normal mode, depicted in Figure 3, was excited to an energy equal to the experimental fundamental (see below). We

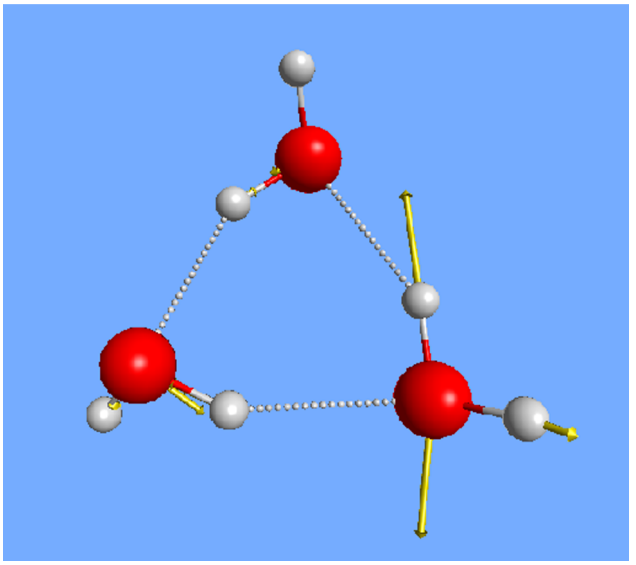

Figure 3. Depiction of the H-bonded OH-stretch (mass-scaled) normal mode that is excited.

use the experimental energy instead of the harmonic one; the difference between the two is roughly 100 cm^{-1}.[42] The normal mode coordinates and momenta were sampled randomly subject to the given mode energy. The transformation from normal coordinates and momenta to standard Cartesian coordinates and momenta was then done, followed by a small purification that subtracted any residual angular velocity in the Cartesian coordinate and momenta to have zero total angular momentum at t = 0 to ensure zero total angular momentum. Then the trajectories were propagated in Cartesian coordinates using the Verlet propagator with a time step of 0.1 fs. A total of roughly 25 000 trajectories were propagated using the WHBB PES.[42] Of these, roughly 20 000 dissociated to a monomer plus dimer. The dissociation criterion was based on the distance of the second largest OO being at least 10 bohr. We chose the second largest distance to ensure that dissociation occurred. Final product analysis was done in the standard way. The internal energy and rotational angular momenta of the dimer and monomer were determined as well as the relative translational energy of the fragments. As we discuss below, the trimer complex is long-lived before dissociating and thus there is significant energy relaxation over most, if not all, the vibrational modes. This suggests that the harmonic description of initial conditions is not a major concern. This long lifetime also offers some justification in using a quasiclassical trajectory approach, instead of quantum one (which is not feasible) as quantum coherence is likely not significant for such long-lived complexes.

RESULTS AND DISCUSSION

The fundamental transition of the H-bonded OH-stretch of $(H_2O)_3$ has previously been assigned and characterized in gas phase, He droplets and inert matrix environments.[21,22,26,28,29] In the gas phase molecular beam experiment, Huisken et al.[21] assigned the H-bonded OH-stretch fundamentals of $(H_2O)_2$, $(H_2O)_3$, and $(H_2O)_4$ at 3601, 3533, and 3416 cm^{-1}, respectively. The observed bands are well isolated and red-

dx.doi.org/10.1021/jp401155v | J. Phys. Chem. A XXXX, XXX, XXX−XXX

shifted by >50 cm^{-1} from the H_2O monomer stretch. The trimer band appears with a broad shoulder to the blue (3552 cm^{-1}), assigned by Paul et al. as a higher cluster band.[22] This has recently been confirmed as the double donor absorption of the hexamer,[29] whose intensity diminishes under conditions where larger clusters are disfavored. There is a tendency to create higher clusters with high backing pressure and high water vapor concentration.[22] Therefore, in our experiments the expansion conditions are carefully optimized to minimize higher cluster formation. In addition, the IR radiation fluence is kept sufficiently low to minimize multiphoton absorption. These optimizations, though reducing signal-to-noise levels, ensure that the detected H_2O fragments are produced from a single photon absorption of the $(H_2O)_3$ species. The signal is further reduced by the large number of accessible fragment monomer states and upper state predissociation of the H_2O REMPI state.[44]

For REMPI spectra and VMI measurements, the H-bonded OH-stretch of $(H_2O)_3$ is excited at 3536 cm^{-1}, which is sufficient only to induce $(H_2O)_3 \rightarrow H_2O + (H_2O)_2$ dissociation. The H_2O fragments are detected state-selectively by REMPI. IR enhancement in the REMPI spectra (IR on−IR off) can be observed only when there is absorption of IR radiation by the trimer that leads to production of H_2O fragments in the monitored J''_{KaKc} level. The signal enhancement in the spectral region where the trimer absorbs ensures that the observed products are produced from VP of $(H_2O)_3$ and not from other clusters. Due to their rotational envelopes, it is impossible to distinguish, with our experimental resolution, between the two types of H-bonds in $(H_2O)_3$, which differ in energy by 12−15 cm^{-1}.[19,28] It is therefore believed that the detected H_2O monomer fragments are formed by breaking of both types of H-bonds.

Little is known about the lifetime of $(H_2O)_3$ excited to the H-bonded OH-stretch. In the He droplet spectrum, the trimer's absorption peak appears slightly broader than the dimer's peak (the dimer's lifetime is 80 ps).[26,49] The calculated lifetime is discussed below.

Figure 4 shows the fragment yield REMPI spectrum of H_2O fragments in the $\tilde{C}\ ^1B_1(000) \leftarrow \tilde{X}\ ^1A_1(000)$ band produced by VP of $(H_2O)_3$ at 3536 cm^{-1}. The spectrum is simulated fairly well with a rotational temperature of 230 ± 70 K, which gives an average energy in rotation of 160 ± 50 cm^{-1}. Upon VP, the estimated excess energy of 810 cm^{-1} (3536−2726 cm^{-1}) can

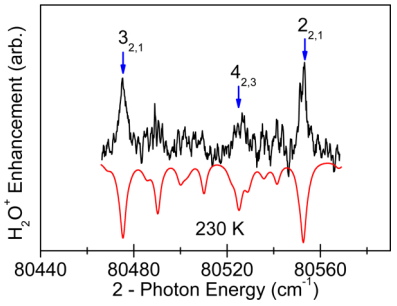

Figure 4. Fragment yield rotational spectrum of $(H_2O)_3$. The top (black) curve corresponds to the fragments 2 + 1 REMPI enhancement spectrum obtained by scanning the H_2O $\tilde{C}\ ^1B_1(000) \leftarrow \tilde{X}\ ^1A_1(000)$ band. The bottom (red) curve shows a PGOPHER[45] simulation with known spectroscopic parameters[44] at 230 K rotational temperature. Assigned REMPI transitions selected for imaging are labeled.

populate H_2O fragment rotational levels up to $J'' = 8$ (or $J''_{KaKc} = 7_{2,5}$). Several isolated rotational transitions ($J'_{KaKc} \leftarrow J''_{KaKc} = 2_{0,2} \leftarrow 2_{2,1}$, $2_{0,2} \leftarrow 3_{2,1}$ and $4_{0,4} \leftarrow 4_{2,3}$) of H_2O fragments were used for imaging. From the rotational temperature of background H_2O in the molecular beams determined from the $\tilde{C}\ ^1B_1(000) \leftarrow \tilde{X}\ ^1A_1(000)$ REMPI spectrum, we estimate the parent trimer temperature at 14 ± 5 K.

Figure 5 shows speed distributions obtained by VMI by monitoring specific rotational states of the H_2O fragments.

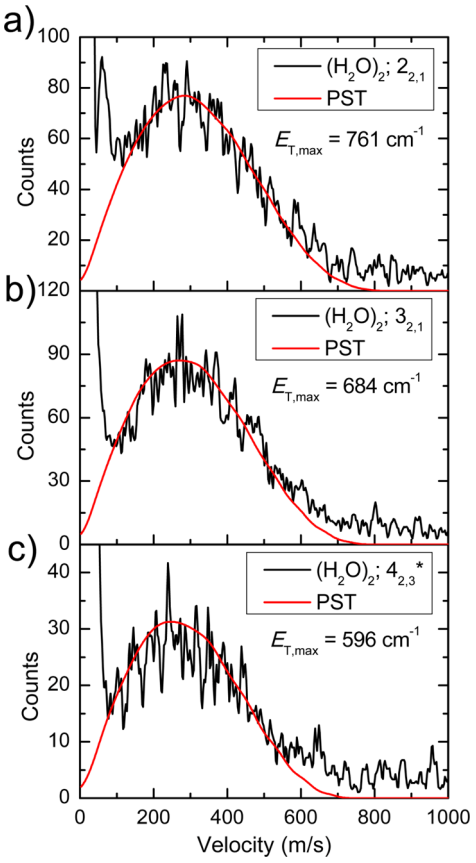

Figure 5. Speed distributions from reconstructed images obtained by monitoring H_2O fragments in J''_{KaKc} = (a) $2_{2,1}$, (b) $3_{2,1}$, and (c) $4_{2,3}$* levels with E_{rot} = 135, 212, and 300 cm^{-1}, respectively. Black curves show experimental measurements, and red curves correspond to the total integrated simulations obtained by using phase space theory (PST, which assumes that all energetically allowed states that conserve angular momentum are equally probable) with D_0 = 2640 cm^{-1} and a resolution of 44 m/s. In (c) $4_{2,3}$* denotes a blended transition with a major contribution from $J''_{KaKc} = 4_{2,3}$. The extended population beyond ∼550 m/s may be due to a contribution from the nearby transition $4_{4,0}$ whose energy is 222 cm^{-1}.

Note that in Figure 5c, the $4_{2,3}$ level has a minor contribution from the $4_{0,4}$ level, which has a lower rotational energy. The recorded two-dimensional projections of ionized H_2O fragments were reconstructed to three-dimensional images as described above. Reconstructed images in speed (velocity) space (m/s) were obtained by summing over the isotropic angular distribution for each radius. The isotropy of the angular distributions reflects the slowness of the dissociation processes. In contrast to the speed distributions obtained in the VP of H_2O and D_2O dimers, as well as water dimers with other small molecules,[34,35,39−41] which show distinct structures in the speed distributions, the speed distributions in Figure 5 are smooth

dx.doi.org/10.1021/jp401155v | J. Phys. Chem. A XXXX, XXX, XXX−XXX

and do not exhibit reproducible structural features. In determining the precise value for D_0 of dimers, we were able to fit distinct and state-specific structures in several speed distributions. In the trimer case, we do not have such structures to rely on, and therefore our estimated value is less precise (see below). The difficulty in estimating D_0 is augmented by the small number of isolated water monomer levels available for imaging. Note that the large fragment signal near zero velocity is associated with background water in the monitored rotational level.

In studies of the VP of the water dimer,[35] it has been shown that the product energy distributions are nonstatistical and generally agree with the energy gap law,[50] resulting in a propensity to populate fragment vibration over rotation over translation. Thus, water monomer fragments with bending excitation were favored over ground state products, and fits to the data demonstrated that the rotational population decreased with increasing translational energy release. As mentioned above, product energy distributions in VP of $(H_2O)_3$ are likely to be more statistical due to the large density of states in the dimer fragment intermolecular vibrational modes, and therefore we decided to compare the measured distributions to simulations using the statistical phase space theory (PST),[51−54] as well as to QCT calculations. In the PST calculations D_0 was the only parameter used in the fits, and we selected a value that best fit both the shapes of the distributions and their cutoff values.

Fitting was accomplished by assigning a Gaussian-shaped curve to rotational levels of each $(H_2O)_2$ cofragment vibrational state, as we have done before.[34,35,39−41] The positions of these Gaussians were determined by conservation of energy,

$$h\nu_{IR} + E_{rot}(\text{trimer}) = D_0 + E_{rot}(\text{mon}) + E_{vib,rot}(\text{dimer}) + E_T$$

where E_{rot}(trimer) is the trimer rotational energy estimated from the IR spectra and beam temperature (10 ± 10 cm^{-1}; because there may be a difference in the cooling efficiency of H_2O and $(H_2O)_3$, the uncertainty of the internal energy is higher), $h\nu_{IR}$ is the IR photon energy (3536 cm^{-1}), E_T is the measured center-of-mass (c.m.) translational energy (proportional to speed^2), and E_{rot}(mon) and $E_{vib,rot}$(dimer) are the rotational energies of the monitored H_2O fragment and the rovibrational energies of the $(H_2O)_2$ cofragment, respectively. E_{rot}(mon) is defined by the selected REMPI transition. Vibrational energies of $(H_2O)_2$ were determined by using the harmonic approximation and the fundamental frequencies from ab initio calculations.[43] The rotational energies were generated by PGOPHER[45] using known rotational constants.[55,56] For H_2O in J''_{KaKc}= $2_{2,1}$, $3_{2,1}$, and $4_{2,3}$, $(H_2O)_2$ cofragments are allowed up to J''_{KaKc} = $60_{1,60}$, $57_{0,57}$, and $53_{1,53}$, respectively. The widths of the Gaussians (full width at half-maximum of 44 m/s) were obtained from previous calibration experiments.[39]

Population distributions were calculated using PST, which assumes that all energetically allowed states that conserve angular momentum are equally probable.[51−54] The vibrational densities of states in the $(H_2O)_2$ cofragment were calculated by the Beyer−Swinehart algorithm.[54,57] All pair-correlated translational energy distributions show energy distribution profiles that vary smoothly with no unique structures in the images. The translational energy distributions were converted to speed distributions and each rovibrational level in the simulation was assigned a Gaussian width of 44 m/s. A best fit D_0 and uncertainty were obtained for each image. Taking a weighted average of all our data, we arrive at a value of D_0 = 2640 ± 140 cm^{-1}. Adding the $(H_2O)_3$ internal energy of 10 ± 10 cm^{-1} yields a final value of D_0 = 2650 ± 150 cm^{-1}. There are two major sources of uncertainty: (1) 140 cm^{-1} obtained from fitting the shapes and cutoffs of the images; (2) 10 cm^{-1} obtained from the internal energy correction. The experimental estimate of D_0 is in good agreement with the calculated value of 2726 ± 30 cm^{-1}.[38] Therefore, a cooperative (nonadditive) effect of 450−500 cm^{-1} is indeed involved in stabilizing the cyclic structure of $(H_2O)_3$.

The good agreement between the measured and calculated D_0 for the water dimer and trimer lends confidence in the high accuracy of the ab initio calculations for D_0 for breaking all three H-bonds of $(H_2O)_3$, which is 3855 ± 20 cm^{-1}. This value is 1129 cm^{-1} higher than the calculated value for breaking two H-bonds. This difference is similar to the value of breaking the single H-bond of $(H_2O)_2$ (1104 ± 5 cm^{-1}), indicating that the cooperative effect is in fact dominated by the cyclic structure and the $(H_2O)_3 \rightarrow H_2O + (H_2O)_2$ dissociation channel.

Although the agreement of the speed distributions with PST is good, it is by no means unique. We can get equally good fits by assuming models in which the rotational distributions obey the energy gap law, i.e., are described with smooth population functions, e^{-CE_T} (where C is a fitting parameter), in which the rotational population decreases with increasing translational energy, and the vibrational distributions have several different forms (see details in Supporting Information). We can, however, confirm the statistical nature of the observed distributions by comparing them to the QCT calculations. The QCT translational energy distribution was calculated using several established methods to account for the ZPE constraint in the fragments. The results, including one with no constraint, all show a peak at around 50 cm^{-1} or less. The major difference among the methods is in the high-energy tail of the distribution. The one shown below was obtained with "hard zero-point constraint", that is, by processing only those trajectories where the monomer and dimer each has at least the respective (harmonic) ZPE. Figure 6 shows a comparison between the measured c.m. translational energy distribution obtained in VMI by detecting H_2O fragments in the J''_{KaKc} = $3_{2,1}$ level and the distributions obtained by QCT calculations where the H_2O fragments are in J'' = 2−4. These rotational levels have a maximum population, and thus a fairly large number of trajectories are associated with them, thereby improving

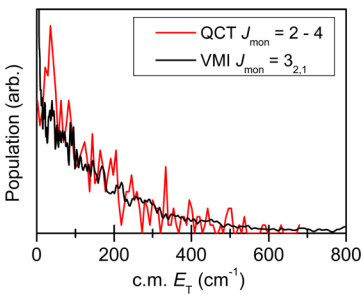

Figure 6. Comparison of the c.m. translational energy distribution measured by VMI by detecting H_2O fragment in the J''_{KaKc} = $3_{2,1}$ level (black curve) and calculated by QCT (hard ZPE constraint), where H_2O fragments are in J'' = 2−4 (red curve).

dx.doi.org/10.1021/jp401155v | J. Phys. Chem. A XXXX, XXX, XXX−XXX

statistics. The agreement between theory and experiment is good.

Figure 7 shows the (hard ZPE constraint) QCT results for the total rotational and translational energy distributions in the

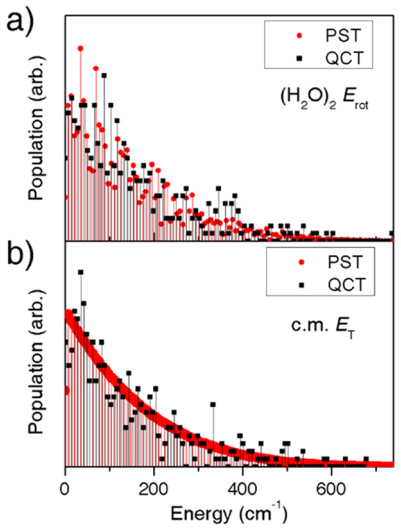

Figure 7. Comparison of $(H_2O)_2$ (a) rotational and (b) translational energy distributions, where the H_2O fragments are in J'' = 2–4, obtained from QCT (hard ZPE constraint) and PST calculations.

$(H_2O)_2$ dimer fragment and compares them with the PST predictions. Note that the energy distributions calculated by using QCT have not been quantized, whereas the PST calculations are quantized and are presented normalized to the total number of trajectories. All PST and QCT distributions agree fairly well, confirming the statistical nature of the energy distributions. Table 1 shows the average vibrational, rotational,

Table 1. Average Vibrational, Rotational, and Translational Energies (cm^{-1}) Obtained from QCT (Hard ZPE Constraint) Calculations and PST (Correlated with J'' = 2–4 of the H_2O Monomer Fragment)

	QCT calculations	PST	temp fit[a]
$(H_2O)_2$ vibration (J'' = 2–4)	342	412	
$(H_2O)_2$ rotation (J'' = 2–4)	151	145	
H_2O rotation (all J'')	229		160 ± 50
translation (J'' = 2–4)	143	142	

[a]The average rotational energy of the H_2O fragment (all J'') obtained from temperature fit is also listed.

and translational energies obtained from the QCT calculations, PST for the $(H_2O)_2$ fragment, and a Boltzmann temperature fit (in cm^{-1}) to the measured rotational distribution of the monomer fragment. All average energies, except the vibrational energy, are in good agreement. Quantizing the vibrational energy distributions calculated from QCT will exclude energetically forbidden states at low energy, which will increase the average vibrational energy and get a result closer to PST.

It is evident that the translational energy release can be well fit by PST as well as by the QCT calculations. In addition, the QCT calculations suggest a statistical-like distribution in the other degrees of freedom. This result is easily rationalized by the large vibrational density of states in the $(H_2O)_2$ fragment. The harmonic intermolecular vibrational energies of the dimer range from 90 to ~600 cm^{-1}, with 4 of the 6 intermolecular vibrational modes being below 300 cm^{-1}.[42,43] The density of vibrational states can reach >8 /cm^{-1} for $(H_2O)_2$ fragments with low rotational and translational energies (see Supporting Information).

As mentioned previously, the product energy distributions in VP of the water dimer are nonstatistical and agree with the energy gap law.[35] For $(H_2O)_3$, the product energy distributions are more statistical due to the large density of states of the products. For future experiments, it will be interesting to examine and compare the energy distributions of the $(H_2O)_3$ → 3 H_2O dissociation channel. Are product energy distributions less statistical due to the lower product density of states? The experimental work cannot distinguish between a mechanism in which the H-bonds are broken sequentially, or several bonds are broken simultaneously; however, the QCT calculations can shed light on this (see below).

Next consider the internal and rotational distributions of the dimer and monomer obtained by QCT. It is worth examining these using the various ZPE constraints (and also no constraint), and so we show results with the indicated constraints and also with no constraints. Figure 8 shows the internal energy of the dimer. With no constraint the distribution is quite broad with about 30% of trajectories leading to the dimer with less than the (harmonic) ZPE. A very similar distribution is seen for the "soft ZPE" constraint, in which the sum of internal energies of the fragments must be at least the sum of the ZPEs. Hard constraints on either the

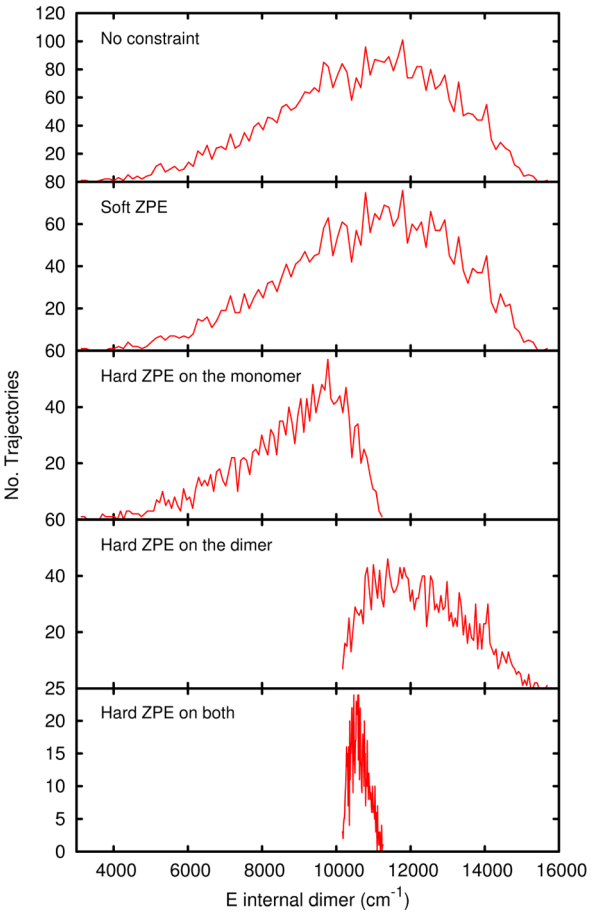

Figure 8. Internal energy of the dimer under indicated treatments of zero-point energy (ZPE). The harmonic ZPE of the dimer is 10 157 cm^{-1}. See text for details of the various ZPE constraints.

dx.doi.org/10.1021/jp401155v | J. Phys. Chem. A XXXX, XXX, XXX–XXX

monomer or the dimer basically "slice" the no-constraint distribution in the expected ways. Finally, the hard-constraint produces a fairly narrow distribution, which shows a peak at around 400 cm^{-1} above the dimer ZPE. There are intermolecular modes in the dimer with harmonic frequencies below 400 cm^{-1} (ref 42, for example), and so we predict that some internal excitation of these dimer modes is likely. (The large reduction in the number of accepted trajectories for the hard-constraint condition compared to the "no-constraint" case implies that many trajectories need to be run and this underscores the need to have an analytical PES available for the calculations.)

Figure 9 shows the dimer rotational angular momentum distribution for the various treatments of the ZPE. In this case,

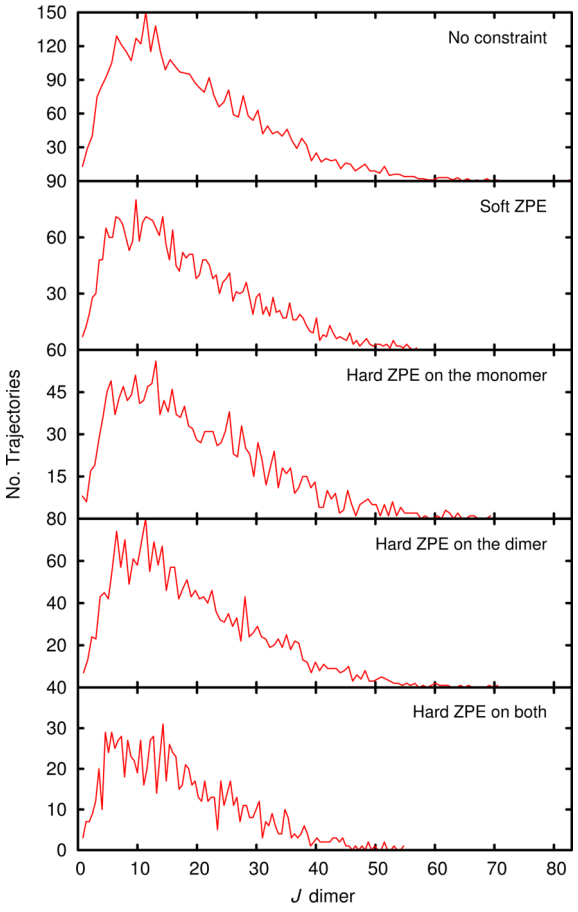

Figure 9. Rotational angular momentum of the dimer under indicated treatments of zero-point energy (ZPE). See text for details of the various ZPE constraints.

as was noted above for the translational energy distribution, there is much less sensitivity on how the ZPE is treated compared to the internal (mostly vibrational) energy distribution of the dimer. As seen, the J distribution is fairly broad with a maximum in the range 10−15. The corresponding distribution for the monomer is shown in Figure 10, where the maximum is predicted to be at roughly 4. (We do not show the monomer vibrational distribution because with the hard constraint there is not sufficient internal energy to excite any normal mode, based on any standard histogram method to assign excited quantum states to classical energy.) In the experiment (Figure 4), we observed water monomer fragments

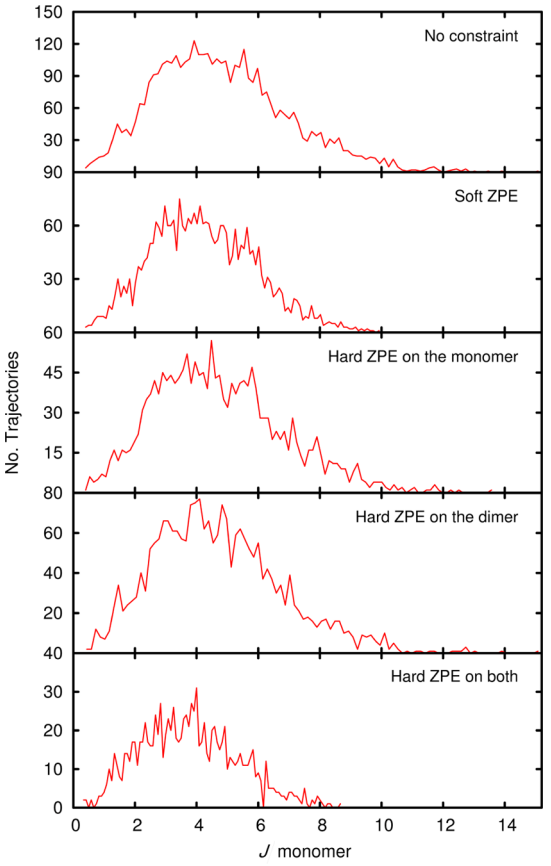

Figure 10. Rotational angular momentum distribution of the monomer under indicated treatments of zero-point energy (ZPE). See text for details of the various ZPE constraints.

mostly in rotational levels J'' = 2−5, which agrees with the QCT calculations.

The trajectories show, as expected, much internal isomerization of the trimer prior to dissociation. Snapshots of one trajectory, shown in Figure 11, illustrate this. The full animation in mpg format is available. Inspection of the trajectories tells us that the ring opens early in the trajectory, indicating the breaking of one H-bond. It re-forms and breaks and re-forms and breaks (often with different H-bonds breaking) until finally the second H-bond breaks and fragmentation is seen. The evolution described by the water trimer trajectories is similar to what was inferred from spectroscopic studies of trimers of HF,[58] DF,[59] and HCl.[60] In these studies it was concluded that the first step in the dissociation is opening of the ring, followed by further intramolecular vibrational redistribution and finally elimination of a monomer fragment. The time scales, however, differ from case to case, reflecting differences in ring strain, vibrational levels, etc.

Finally, to obtain an estimate of the QCT lifetime of dissociation to the dimer + monomer, we simply kept track of the three OO distances and used the dissociation criterion mentioned above to record the time for dissociation. From the distribution of lifetimes for nearly 20 000 trajectories (with no constraints) that dissociated, 84% did so within 10.5 ps. This is shorter than the reported comparable percentage for the water dimer (using the same PES) following OH-stretch excitation, which was reported as "At 25 ps about 84% of the $(H_2O)_2$ trajectories dissociated".[35] It must be noted that the criterion for dissociation in the two cases are not identical but certainly

dx.doi.org/10.1021/jp401155v | J. Phys. Chem. A XXXX, XXX, XXX−XXX

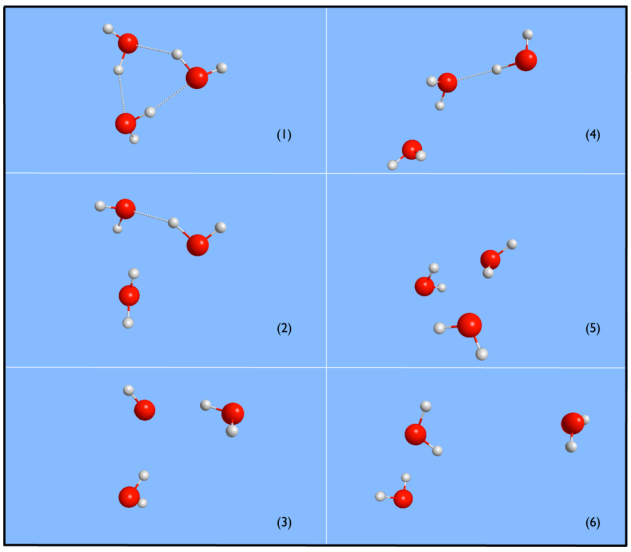

Figure 11. Snapshots of a trajectory (~100 ps) of an initially excited trimer (1) (as described in the text) that dissociates to the dimer + monomer depicted in (6). (2)−(5) depict the intermediate (in increasing time) distortions of the trimer including a nearly linear configuration (4) and compressed re-formed trimer (5). The full animation in mpg format is available.

comparable, and differences between them would account for a fraction of a picosecond uncertainty in the comparisons.

SUMMARY AND CONCLUSIONS

The present joint experimental-theoretical study of the VP of the water trimer provides the first experimental determination of D_0 of the trimer upon excitation of the H-bonded OH stretch fundamental, and an estimation of the contributions of cooperative interactions to the H-bonding network. The experimental value, $D_0 = 2650 \pm 150$ cm^{-1} for $(H_2O)_3 \rightarrow H_2O + (H_2O)_2$, derived from fitting images of selected rotational levels of the water monomer fragment, agrees well with the calculated value ($D_0 = 2726 \pm 30$ cm^{-1}), and places the cooperative contribution for this channel at about 450 cm^{-1}, again in good agreement with theory. It appears, therefore, that most of the cooperativity is captured by breaking off one water molecule from the cyclic trimer.

The QCT calculations provide the first description of the dissociation mechanism of the trimer. The trajectories show that the trimer lives on average for >10 ps before dissociating, allowing ample time for intramolecular vibrational energy redistribution. Indeed, complex vibrational motions are observed that include, among others, isomerization of the H-bonded and free hydrogens, partial breaking and re-formation of H-bonds, etc. The trajectories show that the ring opens first by breaking one H-bond, and after many subsequent vibrational motions, the second bond breaks as well, liberating a water monomer.

In addition, the QCT calculations provide the c.m. translational energy distribution, as well as the rotational energy distributions in the monomer and dimer fragments. Good agreement is obtained between the QCT calculations and PST predictions, as well as with the experimentally measured pair-correlated speed distributions. We conclude that the fairly long dissociation times and large density of states leads to statistical-like energy distributions. A nearly statistical outcome is also in accordance with what is seen in the trajectories, which favor a mechanism in which most dissociation events involve stepwise H-bond breaking, facilitating energy redistribution among the intermolecular vibrations of the dimer and the reaction coordinate.

The statistical-like behavior of the VP of the water trimer stands in contrast to the corresponding behavior of the water dimer, in which the fragment rovibrational energy distributions are nonstatistical even though the dimer's lifetime is longer than the trimer's. The difference can be attributed partly to the existence of low-lying (<300 cm^{-1}) intermolecular vibrational levels in the dimer fragment that facilitate energy transfer in the trimer. We do not know whether the dimer fragment vibrational energy distribution is statistical but the QCT calculations show that a large fraction of the available energy is deposited in dimer fragment vibration. We conclude that the energy gap law is not as important in the VP of the trimer as it is for the dimer.

ASSOCIATED CONTENT

Supporting Information

Average vibrational density of states of $(H_2O)_2$; speed distributions and additional simulations. This information is available free of charge via the Internet at http://pubs.acs.org.

Web-Enhanced Feature

Full animation in mpg format of the snapshots in Figure 11 is available in the HTML version of the paper.

AUTHOR INFORMATION

Corresponding Author

*E-mail: reisler@usc.edu (H.R.), jmbowma@emory.edu (J.M.B.).

Notes

The authors declare no competing financial interest.

ACKNOWLEDGMENTS

This work was supported by the U.S National Science Foundation Grants CHE-0951976 (H.R.) and CHE-1145227 (J.M.B.).

REFERENCES

(1) Latimer, W. M.; Rodebush, W. H. Polarity and Ionization from the Standpoint of the Lewis Theory of Valence. *J. Am. Chem. Soc.* **1920**, *42*, 1419−1433.

(2) Pauling, L. The Shared-Electron Chemical Bond. *Proc. Natl. Acad. Sci. U. S. A.* **1928**, *14*, 359−362.

(3) Pauling, L. *The Nature of the Chemical Bond and the Structure of Molecules and Crystals: An Introduction to Modern Structural Chemistry*; Cornell University Press: Ithaca, NY, 1939.

(4) Bernal, J. D.; Fowler, R. H. A Theory of Water and Ionic Solution, with Particular Reference to Hydrogen and Hydroxyl Ions. *J. Chem. Phys.* **1933**, *1*, 515−548.

(5) Scheiner, S. *Hydrogen Bonding: A Theoretical Perspective*; Oxford University Press: New York, 1997.

(6) Keutsch, F. N.; Saykally, R. J. Water Clusters: Untangling the Mysteries of the Liquid, One Molecule at a Time. *Proc. Natl. Acad. Sci. U. S. A.* **2001**, *98*, 10533−10540.

(7) Fowler, J. E.; Schaefer, H. F. III. Detailed Study of the Water Trimer Potential Energy Surface. *J. Am. Chem. Soc.* **1995**, *117*, 446−452.

(8) Xantheas, S. S.; Burnham, C. J.; Harrison, R. J. Development of Transferable Interaction Models for Water. II. Accurate Energetics of the First Few Water Clusters from First Principles. *J. Chem. Phys.* **2002**, *116*, 1493−1499.

(9) Wales, D. J. Theoretical Study of Water Trimer. *J. Am. Chem. Soc.* **1993**, *115*, 11180−11190.
(10) Takahashi, M.; Watanabe, Y.; Taketsugu, T.; Wales, D. J. An ab initio Study of Tunneling Splittings in the Water Trimer. *J. Chem. Phys.* **2005**, *123*, 044302.
(11) Mas, E. M.; Bukowski, R.; Szalewicz, K. Ab initio Three-Body Interactions for Water. I. Potential and Structure of Water Trimer. *J. Chem. Phys.* **2003**, *118*, 4386−4403.
(12) Keutsch, F. N.; Cruzan, J. D.; Saykally, R. J. The Water Trimer. *Chem. Rev.* **2003**, *103*, 2533−2578.
(13) Anderson, J. A.; Crager, K.; Fedoroff, L.; Tschumper, G. S. Anchoring the Potential Energy Surface of the Cyclic Water Trimer. *J. Chem. Phys.* **2004**, *121*, 11023.
(14) Santra, B.; Michaelides, A.; Scheffler, M. On the Accuracy of Density-Functional Theory Exchange-Correlation Functionals for H Bonds in Small Water Clusters: Benchmarks Approaching the Complete Basis Set Limit. *J. Chem. Phys.* **2007**, *127*, 184104.
(15) van der Avoird, A.; Szalewicz, K. Water Trimer Torsional Spectrum from Accurate ab initio and Semiempirical Potentials. *J. Chem. Phys.* **2008**, *128*, 014302.
(16) Kiss, P. T.; Baranyai, A. Clusters of Classical Water Models. *J. Chem. Phys.* **2009**, *131*, 204310.
(17) Salmi, T.; Kjaergaard, H. G.; Halonen, L. Calculation of Overtone O−H Stretching Bands and Intensities of the Water Trimer. *J. Phys. Chem. A* **2009**, *113*, 9124−9132.
(18) Czakó, G.; Kaledin, A. L.; Bowman, J. M. Zero-Point Energy Constrained Quasiclassical, Classical, and Exact Quantum Simulations of Isomerizations and Radial Distribution Functions of the Water Trimer Using an ab Initio Potential Energy Surface. *Chem. Phys. Lett.* **2010**, *500*, 217−222.
(19) Salmi, T.; Sälli, E.; Halonen, L. A Nine-Dimensional Calculation of the Vibrational OH Stretching and HOH Bending Spectrum of the Water Trimer. *J. Phys. Chem. A* **2012**, *116*, 5368−5374.
(20) Pugliano, N.; Saykally, R. J. Measurement of Quantum Tunneling Between Chiral Isomers of the Cyclic Water Trimer. *Science* **1992**, *257*, 1937−1940.
(21) Huisken, F.; Kaloudis, M.; Kulcke, A. Infrared Spectroscopy of Small Size-Selected Water Clusters. *J. Chem. Phys.* **1996**, *104*, 17−25.
(22) Paul, J. B.; Collier, C. P.; Saykally, R. J.; Scherer, J. J.; O'Keefe, A. Direct Measurement of Water Cluster Concentrations by Infrared Cavity Ringdown Laser Absorption Spectroscopy. *J. Phys. Chem. A* **1997**, *101*, 5211−5214.
(23) Braly, L. B.; Liu, K.; Brown, M. G.; Keutsch, F. N.; Fellers, R. S.; Saykally, R. J. Terahertz Laser Spectroscopy of the Water Dimer Intermolecular Vibrations. II. $(H_2O)_2$. *J. Chem. Phys.* **2000**, *112*, 10314−10326.
(24) Braly, L. B.; Cruzan, J. D.; Liu, K.; Fellers, R. S.; Saykally, R. J. Terahertz Laser Spectroscopy of the Water Dimer Intermolecular Vibrations. I. $(D_2O)_2$. *J. Chem. Phys.* **2000**, *112*, 10293−10313.
(25) Keutsch, F. N.; Braly, L. B.; Brown, M. G.; Harker, H. A.; Petersen, P. B.; Leforestier, C.; Saykally, R. J. Water Dimer Hydrogen Bond Stretch, Donor Torsion Overtone, and "In-Plane Bend" Vibrations. *J. Chem. Phys.* **2003**, *119*, 8927−8937.
(26) Slipchenko, M. N.; Kuyanov, K. E.; Sartakov, B. G.; Vilesov, A. F. Infrared Intensity in Small Ammonia and Water Clusters. *J. Chem. Phys.* **2006**, *124*, 241101.
(27) Ceponkus, J.; Uvdal, P.; Nelander, B. Far-Infrared Band Strengths in the Water Dimer: Experiments and Calculations. *J. Phys. Chem. A* **2008**, *112*, 3921−3926.
(28) Burnham, C. J.; Xantheas, S. S.; Miller, M. A.; Applegate, B. E.; Miller, R. E. The Formation of Cyclic Water Complexes by Sequential Ring Insertion: Experiment and Theory. *J. Chem. Phys.* **2002**, *117*, 1109−1122.
(29) Moudens, A.; Georges, R.; Goubet, M.; Makarewicz, J.; Lokshtanov, S. E.; Vigasin, A. A. Direct Absorption Spectroscopy of Water Clusters Formed in a Continuous Slit Nozzle Expansion. *J. Chem. Phys.* **2009**, *131*, 204312.
(30) Mó, O.; Yáñez, M.; Elguero, J. Cooperative (Nonpairwise) Effects in Water Trimers: An ab initio Molecular Orbital Study. *J. Chem. Phys.* **1992**, *97*, 6628−6638.
(31) González, L.; Mó, O.; Yáñez, M.; Elguero, J. Cooperative Effects in Water Trimers. The Performance of Density Functional Approaches. *J. Mol. Struc. (THEOCHEM)* **1996**, *371*, 1−10.
(32) Glendening, E. D. Natural Energy Decomposition Analysis: Extension to Density Functional Methods and Analysis of Cooperative Effects in Water Clusters. *J. Phys. Chem. A* **2005**, *109*, 11936−11940.
(33) Ohno, K.; Okimura, M.; Akai, N.; Katsumoto, Y. The Effect of Cooperative Hydrogen Bonding on the OH Stretching-Band Shift for Water Clusters Studied by Matrix-Isolation Infrared Spectroscopy and Density Functional Theory. *Phys. Chem. Chem. Phys.* **2005**, *7*, 3005−3014.
(34) Rocher-Casterline, B. E.; Ch'ng, L. C.; Mollner, A. K.; Reisler, H. Communication: Determination of the Bond Dissociation Energy D_0 of the Water Dimer, $(H_2O)_2$, by Velocity Map Imaging. *J. Chem. Phys.* **2011**, *134*, 211101.
(35) Ch'ng, L. C.; Samanta, A. K.; Czakó, G.; Bowman, J. M.; Reisler, H. Experimental and Theoretical Investigations of Energy Transfer and Hydrogen-Bond Breaking in the Water Dimer. *J. Am. Chem. Soc.* **2012**, *134*, 15430−15435.
(36) Shank, A.; Wang, Y.; Kaledin, A.; Braams, B. J.; Bowman, J. M. Accurate ab initio and "Hybrid" Potential Energy Surfaces, Intramolecular Vibrational Energies, and Classical IR Spectrum of the Water Dimer. *J. Chem. Phys.* **2009**, *130*, 144314.
(37) Czakó, G.; Bowman, J. M. Quasiclassical Trajectory Calculations of Correlated Product Distributions for the F + $CHD_3(v_1 = 0,1)$ Reactions Using an ab initio Potential Energy Surface. *J. Chem. Phys.* **2009**, *131*, 244302.
(38) Wang, Y.; Bowman, J. M. Communication: Rigorous Calculation of Dissociation Energies (D_0) of the water trimer, $(H_2O)_3$ and $(D_2O)_3$. *J. Chem. Phys.* **2011**, *135*, 131101.
(39) Rocher-Casterline, B. E.; Mollner, A. K.; Ch'ng, L. C.; Reisler, H. Imaging H_2O Photofragments in the Predissociation of the HCl−H_2O Hydrogen-Bonded Dimer. *J. Phys. Chem. A* **2011**, *115*, 6903−6909.
(40) Casterline, B. E.; Mollner, A. K.; Ch'ng, L. C.; Reisler, H. Imaging the State-Specific Vibrational Predissociation of the Hydrogen Chloride−Water Hydrogen-Bonded Dimer. *J. Phys. Chem. A* **2010**, *114*, 9774−9781.
(41) Mollner, A. K.; Casterline, B. E.; Ch'ng, L. C.; Reisler, H. Imaging the State-Specific Vibrational Predissociation of the Ammonia Water Hydrogen-Bonded Dimer. *J. Phys. Chem. A* **2009**, *113*, 10174−10183.
(42) Wang, Y.; Shepler, B. C.; Braams, B. J.; Bowman, J. M. Full-Dimensional, ab initio Potential Energy and Dipole Moment Surfaces for Water. *J. Chem. Phys.* **2009**, *131*, 054511.
(43) Kalescky, R.; Zou, W.; Kraka, E.; Cremer, D. Local Vibrational Modes of the Water Dimer − Comparison of Theory and Experiment. *Chem. Phys. Lett.* **2012**, *554*, 243−247.
(44) Yang, C. H.; Sarma, G.; ter Meulen, J. J.; Parker, D. H.; Western, C. M. REMPI Spectroscopy and Predissociation of the $\tilde{C}^1B^1(v = 0)$ Rotational Levels of H_2O, HOD and D_2O. *Phys. Chem. Chem. Phys.* **2010**, *12*, 13983−13991.
(45) Western, C. M. *PGOPHER 2010, a Program for Simulating Rotational Structure*; University of Bristol, http://pgopher.chm.bris.ac.uk.
(46) Eppink, A. T. J. B.; Parker, D. H. Velocity Map Imaging of Ions and Electrons Using Electrostatic Lenses: Application in Photoelectron and Photofragment Ion Imaging of Molecular Oxygen. *Rev. Sci. Instrum.* **1997**, *68*, 3477−3484.
(47) Dribinski, V.; Potter, A. B.; Fedorov, I.; Reisler, H. Two-Photon Dissociation of the NO Dimer in the Region 7.1−8.2 eV: Excited States and Photodissociation Pathways. *J. Chem. Phys.* **2004**, *121*, 12353.
(48) Dribinski, V.; Ossadtchi, A.; Mandelshtam, V. A.; Reisler, H. Reconstruction of Abel-Transformable Images: The Gaussian Basis-Set

Expansion Abel Transform Method. *Rev. Sci. Instrum.* **2002**, *73*, 2634−2642.
(49) Paul, J. B.; Provencal, R. A.; Chapo, C.; Petterson, A.; Saykally, R. J. Infrared Cavity Ringdown Spectroscopy of Water Clusters: O-D Stretching Bands. *J. Chem. Phys.* **1998**, *109*, 10201−10206.
(50) Ewing, G. E. Selection Rules for Vibrational Energy Transfer: Vibrational Predissociation of van der Waals Molecules. *J. Phys. Chem.* **1987**, *91*, 4662−4671.
(51) Light, J. C. Phase-Space Theory of Chemical Kinetics. *J. Chem. Phys.* **1964**, *40*, 3221−3229.
(52) Pechukas, P.; Light, J. C. On Detailed Balancing and Statistical Theories of Chemical Kinetics. *J. Chem. Phys.* **1965**, *42*, 3281−3291.
(53) Pechukas, P.; Light, J. C.; Rankin, C. Statistical Theory of Chemical Kinetics: Application to Neutral-Atom-Molecule Reactions. *J. Chem. Phys.* **1966**, *44*, 794−805.
(54) Baer, T.; Hase, W. L. *Unimolecular Reaction Dynamics: Theory and Experiments*; Oxford University Press, Inc.: New York, 1996.
(55) Fraser, G. T. $(H_2O)_2$: Spectroscopy, Structure and Dynamics. *Int. Rev. Phys. Chem.* **1991**, *10*, 189−206.
(56) Zwart, E.; ter Meulen, J. J.; Leo Meerts, W.; Coudert, L. H. The Submillimeter Rotation Tunneling Spectrum of the Water Dimer. *J. Mol. Spectrosc.* **1991**, *147*, 27−39.
(57) Beyer, T.; Swinehart, D. F. Algorithm 448: Number of Multiply-Restricted Partitions. *Commun. ACM* **1973**, *16*, 379.
(58) Michael, D. W.; Lisy, J. M. Vibrational Predissociation Spectroscopy of $(HF)_3$. *J. Chem. Phys.* **1986**, *85*, 2528−2537.
(59) Suhm, M. A.; Farrell, J. J. T.; Ashworth, S. H.; Nesbitt, D. J. High-Resolution Infrared Spectroscopy of DF Trimer: A Cyclic Ground State Structure and DF Stretch Induced Intramolecular Vibrational Coupling. *J. Chem. Phys.* **1993**, *98*, 5985−5989.
(60) Farnik, M.; Nesbitt, D. J. Intramolecular Energy Transfer between Oriented Chromophores: High-Resolution Infrared Spectroscopy of HCl Trimer. *J. Chem. Phys.* **2004**, *121*, 12386.